Available online www.ejaet.com

European Journal of Advances in Engineering and Technology, 2023, 10(7): 20-31

Research Article ISSN: 2394 - 658X

Simultaneous Voltage and Frequency Regulation in Power Grid by a New Control Strategy of Active and Reactive Power Generation

Abdelazim M. Salem, Shrouk O. Ibraheem, M.A.M Abdel Ghany and Amgad E. Salem

Electrical Power Department, October 6th University, 6th of October, Giza, Egypt
abdelazim.salem.eng@o6u.edu.eg, shorouk.eng@o6u.edu.eg, m.a.abdelghany.eng@o6u.edu.eg, amgadaboraya.eng@o6u.edu.eg

---

ABSTRACT

This paper addressed analysis, design and tracking active power flow (APF) while preserving the reactive power flow (RPF) at a desired value for turbo-generator system at the infinite bus. The proposed new methodology is based on the effect of APF and RPF on each other by simultaneously controlling both voltage and frequency in power grid. The system performance has been improved by adding new parameters G_1, G_2, G_3 and G_4 derived by mathematical analysis model of an actual power system. The optimization parameters of fuzzy self-tuning PID (OFSTPID) have been implemented for two loop controllers. The proposed technique has been compared with the conventional method of LFC for [(0.8±0.08) + j0.6]pu. The potential of proposed technique contributed to enhancing the dynamic performance of the system and tracking of active and reactive power flow. Also, the generator has ability to send larger active power than conventional LFC because the power angle of proposed method is smaller than the same APF disturbance. So, the reliability and power quality have been improved. The overall results are compared with related previous works according to dynamic response of frequency deviation and show its superiority over the conventional LFC and combined of LFC and AVR technique.

Key words: Active power flow, Reactive power flow, Turbo-generator, Fuzzy self-tunning.

Nomenclature

Symbols	Variable name	Symbols	Variable name
$\bar{A}$ and $\bar{B}$	constants related to the system configuration	ΔP_∞ and ΔQ_∞	Change in active and reactive power at infinite bus
$\bar{E}_g$	back induced e.m.f.	$T_S(\pm 2\%\ band)$	Settling time
e and Δe	error and change of error	T_P	Peak time.
$\bar{E}_f$	Exciter field voltage response	$U_P(\%)$	Peak undershoot
F_g	Global objective function	U_{tun}	output control action of FSTPID
F_1, F_2, F_3 and F_4	individual objective function	V_{ter}	Generator terminal voltage
, G_2, G_3 and G_1 G_4	Control gain parameters	$\bar{V}_\infty$	Infinite bus voltage
$\bar{I}_\infty$	Infinite bus current	∝	Angle of A constant
$(K_P, K_I, K_D)\_P$	Active OFOPID parameters	B	Angle of B constant
$(K_P, K_I, K_D)\_Q$	Reactive OFOPID parameters	δ	Power angle
$M_P(\%)$	Peak overshoot±2%band	$\propto_Q, \beta_Q, \gamma_Q$ and δ_Q	Scaling factors
P_∞, Q_∞ and S_∞	Active, reactive and apparent power at infinite bus		

1. INTRODUCTION

1. Motivations and incitements

The keeping of nominal values of voltage and frequency in the electrical network are the most important parameters of power quality [1],[2]. To maintain these generated values, the LFC and AVR are adopted. In an actual power system, many researchers relied on approaches for decoupling between LFC and AVR to facilitate the control of active power demand without taking into consideration the deviation of generator voltage[3], [4]. While, other researchers are interested with AVR without taking into consideration the deviation in the generator frequency [5], [6].In general, all researchers who adopt the LFC or AVR have their motivations. But, this paper deals with the variation that occur in the delivered reactive power during the control of the delivered active power. The meeting of active and reactive power demand makes the loads are operating efficiently. While the shortages of active and reactive power demand are negatively impacts on the load efficiency.

1.2 Literature background

To improve the frequency deviation, LFC loop reduces the gap between active power demand and generated active power by controlling the governor valve position. Also, AVR loop reduces the gap between reactive power demand and generated reactive power to regulate the terminal voltage by controlling the exciter field voltage [7]. Recently, the researchers focus on combining of two techniques (LFC-AVR). The combination system of LFC-AVR is carried out on a solar thermal power unit using PI-TID controller [8]. The combined of LFC-AVR is adopted on the hydrothermal power generation under the simulated annealing (SA)based PID controller [9]. In [7], [10], the researchers applied the combined of LFC-AVR on multi-generation stations using IPFC-RFBs control [7] and PID based the moth flame optimizer (MFO) [10]respectively. The authors in [11] are carried out the combination of LFC-AVR to a three-area system with Integral-double derivative controller with derivative filter (IDDF) using a lightening search algorithm (LSA) for each area consists of thermal and diesel unit. It is clear that, most of the published papers dealt with the combined of LFC-AVR technique depending on the different control method or different metaheuristic optimization methods. But this paper has been changed the structure of the control loops by adding the gain parameters G_(1,) G_(2,) G_3 and G_4 that were deduced by mathematical analysis to control APF and RPF at the same time. Due to the interaction and nonlinearity between the active and reactive power, the conventional PID controllers are not extensive supportable.[12]. To overcome this problem, FLC is the one of the preferable methods which applied to PID controller [4], [13]–[15]. This method depend on parameters adjustment of PID gains by using ACO optimization method as a 1st step. Then, the FLC gains are designed by membership functions and fuzzy rules as a 2nd step. The adaptation output parameters of OFSTPID can be determined by multiplying the output gains of PID and FLC. OFSTPID has many advantages over the traditional controllers. It covers a wider range for operating conditions, cheaper for developing, automatically improve an initial approximate set of fuzzy rules[12], [14]. So, fuzzy self-tuning PID(FSTPID) based on ant colony optimization method has been adopted.

1.3 Contribution and Paper Organization

The schematic diagram of proposed control is illustrated in Fig.1 as a real power system. There is a tightly relationship between the governor valve position control loop and field exciter voltage control loopis represented by four gain parameters G_(1,) G_(2,) G_3 and G_4. The evaluation of these gains will be discussed in section 3.

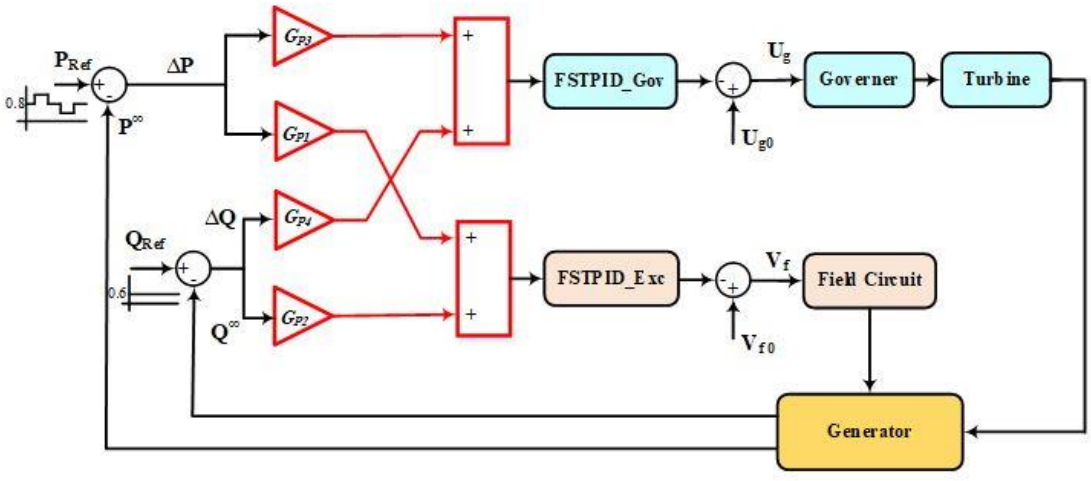

Fig. 1 Reality power system control scheme

- Mathematical model derivation proposed for tracking the APF and preserving the RPF of turbo-generator system at the infinite bus.
- Create the control gain parameters G_(1,) G_(2,) G_3 and G_4to meet the APF and RPF at the infinite bus based mathematical analysis.
    - 6^{th} PID parameters of OFSTPID controller are optimized using ACO for each governor and exciter control loops.
- The generator has ability to send larger active power than the case of conventional LFC because the power angle of proposed method is smaller than by 5.014% at the same APF disturbance
- The system has been tested by ±10% of initial active power demand.
- Performance assessment of proposed system compared with the relevant previous works.

This paper is organized as follows: section 2 defined the problem and section 3
presented the proposed model and analysis of reality system. Section 4 presented the proposed system parameters optimization. In section 5 discussed the results to verify the proposed control scheme and comparative study of previous works. Finally, the conclusions are listed in Section 6.

2. PROBLEM DEFINITION

The LFC technique plays a crucial role to maintain the reliability and stability of power systems by controlling the active power generation according to load variations [12], [16]–[18]. But the reactive power variation is one of the important issues that are affected by LFC. Reactive power variation is a critical concern in power systems because it affects the voltage stability and overall performance of the grid. The voltage instability leads to equipment damage and power system collapse [19]–[21].

Fig. 2 shows that the PID controller response of APF (P_∞) and related parameter curves such as governor position (U_g), power angle (δ) and change in the frequency deviation (Δf) according to conventional LFC technique. Fig. 2a illustrates the reference of active power load curve (P_ref) and the response of P_∞. The initial set point suggested of P_ref at 0.8pu during 0 - 5 seconds and ±10%load disturbance according to set point from5 - 20 second and 35 – 50 respectively. The response of P_∞ has been tracked the desired value after settling time 12.23 second with overshoot (25%) and undershoot (12.5%). In Fig.2b, the steady state value of the governor position increased and deceased by 10.1% from set point where the response of governor valve position is directly proportional to P_∞. Fig. 2c represents the power angle which increased to 53.2° (14.1%) in the interval 5 - 20 second and decreased to 40.75° (12.6%) in the interval 35 - 50 second. Fig.3d shows the frequency deviation response with overshoot and undershoot ±0.0075 Hz (0.00015pu) while its settling time is 9.2 seconds.

Fig. 3a shows that the reference of reactive power load curve (Q_ref) and the response of Q_∞. The initial set point suggested of Q_ref at 0.6pu through 0 - 70 seconds. The RPF has been decreased to 0.525pu (12.5%) from 5-20 seconds while the APF in Fig. 2b increased by 10%. During 35: 50 second, The RPF has been increased to 0.66pu (10%) while the APF in Fig. 3b was decreased by 10%. The disadvantages of the reverse response between RPF and APF leads to decrease the power quality and reliability of power system [22]. Regardless of changing in RPF but, the field excitation voltage response (Ef) still at 2.659pu during the complete time simulation as shown Fig. 3b. Fig. 3c illustrates the response of terminal generator voltage (Vter) has the same response of Q∞. The value of Vter is reduced by 2.1 % from 5-20 seconds and increased by 1.7% from 35-50 seconds.

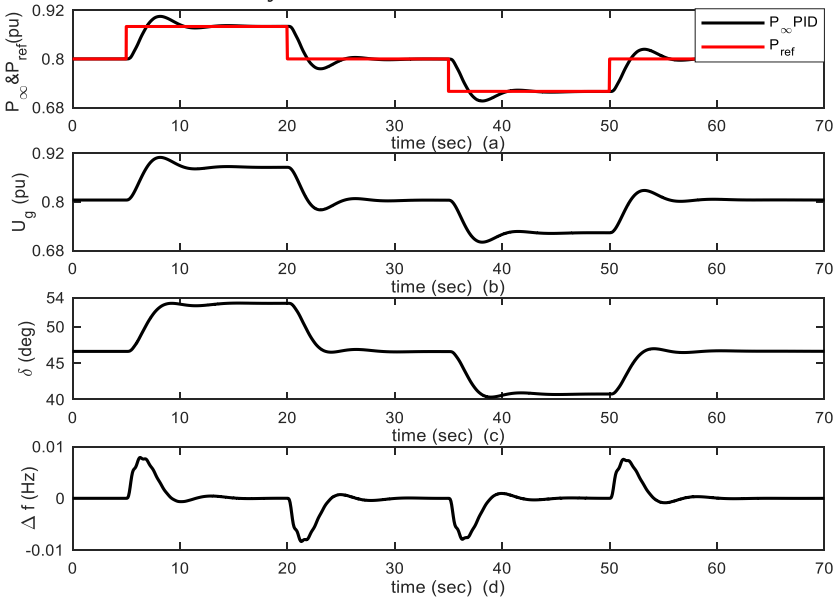

Fig 2: APF and related response of the conventional LFC using PID controller
a-P_∞ & P_ref (pu); -b- U_g; c- δ; d-Δf

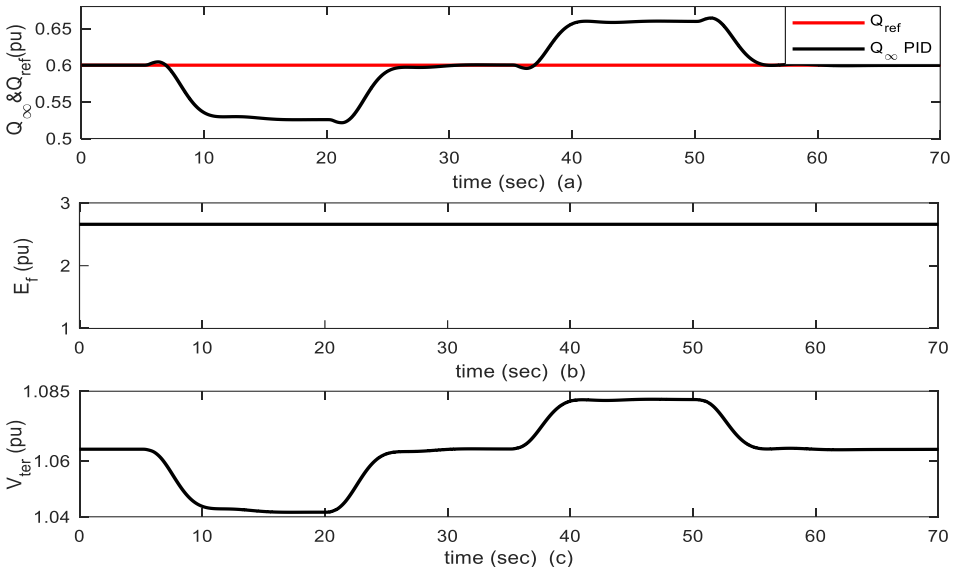

Fig 3: RPF and related response of the conventional LFC for PID controller.
a-Q_∞ & Q_ref; -b- E_f; c- V_ter

3. PROPOSAL OF MODELING AND ANALYSIS OF REALITY POWER SYSTEM

According to simulation results in section 2, it is clear that there is a divergence in the relation between APF and RPF of turbo generator. Therefore, it is essential to establish a correlation between variations in active and reactive power delivered to grid from synchronous generator depends on changing the power angle and the back induced emf in the generator. To meet the active and reactive power demand, authors will adopt the analytical concepts of power systems to deduce the gain parameters that facilitate the controller performance. The realistic power system can be emulated as two-port network as shown in Fig.4. Where E_g is a back induced e.m.f. of synchronous generator, V∞ is a constant voltage source can be taken as a voltage, while A and B are the constants depend on the equivalent circuit for the power system.

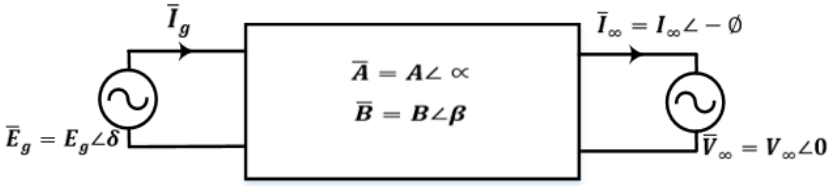

Fig. 4 Two-port network system

According to Fig. 4, the mathematical analysis consists of two proposals:

- The first proposal of mathematical analysis can be written as,

$$\bar{E}_g = \bar{A}\bar{V}_\infty + \bar{B}\bar{I}_\infty \quad (1)$$

$$\bar{I}_\infty = \frac{\bar{E}_g}{\bar{B}} - \frac{\bar{A}}{\bar{B}}\bar{V}_\infty \quad (2)$$

$$\bar{I}^*_\infty = \frac{\bar{E}^*_g}{\bar{B}^*} - \frac{\bar{A}^*}{\bar{B}^*}\bar{V}^*_\infty \quad (3)$$

For per unit system,

$$\bar{S}_\infty = P_\infty + jQ_\infty = \bar{V}_\infty\bar{I}^*_\infty \quad (4)$$

$$\bar{S}_\infty = \frac{\bar{E}^*_g}{\bar{B}^*}\bar{V}_\infty - \frac{\bar{A}^*}{\bar{B}^*}V^2_\infty \quad (5)$$

So,

$$\bar{S}_\infty = \frac{E_g}{B}V_\infty\angle\beta - \delta \ - \frac{A}{B}V^2_\infty\angle\beta - \alpha \quad (6)$$

Then, $P_\infty = \frac{E_g}{B}V_\infty\cos(\beta - \delta) \ - \frac{A}{B}V^2_\infty\cos(\beta - \alpha)$ (7)

$$Q_\infty = \frac{E_g}{B}V_\infty\sin(\beta - \delta) \ - \frac{A}{B}V^2_\infty\sin(\beta - \alpha) \quad (8)$$

For open circuit at infinite bus ($I_\infty = 0$);

$$\bar{A} = \frac{\bar{E}_g}{\bar{V}_\infty} \quad (9)$$

For short circuit at infinite bus ($V_\infty = 0$);

$$\bar{B} = \frac{\bar{E}_g}{\bar{I}_\infty} \quad (10)$$

The active and reactive power in equations (7), (8) contain only two variables, namely δ and E_g because other parameters in the equations are considered constants. Applying the Taylor series to equations (7) and (8);

$$\Delta P_\infty = \frac{\partial P_\infty}{\partial E_g} \Delta E_g + \frac{\partial P_\infty}{\partial \delta} \Delta\delta \quad (11)$$

$$\Delta Q_\infty = \frac{\partial Q_\infty}{\partial E_g} \Delta E_g + \frac{\partial Q_\infty}{\partial \delta} \Delta\delta \quad (12)$$

Taking the partial derivative of equations (7) and (8);

$$\frac{\partial P_\infty}{\partial E_g} = \frac{V_\infty}{\beta}\cos(\beta - \delta) \quad (13)$$

$$\frac{\partial P_\infty}{\partial \delta} = \frac{E_g V_\infty}{\beta}\sin(\beta - \delta) \quad (14)$$

$$\frac{\partial Q_\infty}{\partial E_g} = \frac{V_\infty}{\beta}\sin(\beta - \delta) \quad (15)$$

$$\frac{\partial Q_\infty}{\partial \delta} = -\frac{E_g V_\infty}{\beta}\cos(\beta - \delta) \quad (16)$$

The first proposed analysis of relevant concept can be clarified as:

To make the active power positive value, it must be $\delta < \beta$.So, the trigonometric function of sine and cosine is a positive sign. That means that $\cos(\beta - \delta) = +\text{ve}$ value and $\sin(\beta - \delta) = +\text{ve}$. Then the sign of partial derivative $\frac{\partial P_\infty}{\partial E_g} = +\text{ve}$,$\frac{\partial P_\infty}{\partial \delta} = +\text{ve}$ value,$\frac{\partial Q_\infty}{\partial E_g} = +\text{ve}$ value and $\frac{\partial Q_\infty}{\partial \delta} = -\text{ve}$value**.** Based on these concept**s,** if the magnitude of $E_g$is constant value for conventional LFC and $\delta$is increased due to increase the active power (ΔP). Then, the reactive power from equation (15) will be decreased and vice versa. This explanation coincides the active and reactive power response in Fig. 3c and Fig. 3d.

- The second proposal of the factor estimation G_1, G_2, G_3 and G_4can be deduced by the following equations,

Rewrite equations (11) and equation (12) in other forms

$$\Delta P_\infty = A_1 \Delta E_g + A_2 \Delta\delta \quad (17)$$

$$\Delta Q_\infty = B_1 \Delta E_g + B_2 \Delta\delta \quad (18)$$

Where;

$$A_1 = \frac{\partial P_\infty}{\partial E_g}, A_2 = \frac{\partial P_\infty}{\partial \delta}, B_1 = \frac{\partial Q_\infty}{\partial E_g} \text{ and } B_2 = \frac{\partial Q_\infty}{\partial \delta}$$

The equations 17,18 can be reformed in the matrix form as follows:

$$\begin{bmatrix}\Delta P_\infty \\ \Delta Q_\infty\end{bmatrix} = \begin{bmatrix}A_1 & A_2 \\ B_1 & B_2\end{bmatrix}\begin{bmatrix}\Delta E_g \\ \Delta\delta\end{bmatrix} \quad (19)$$

The change in E_g and in δ can be obtained by inversing the matrix

$$\begin{bmatrix}\Delta E_g \\ \Delta\delta\end{bmatrix} = \frac{1}{A_1B_2 - A_2B_1}\begin{bmatrix}B_2 & -A_2 \\ -B_1 & A_1\end{bmatrix}\begin{bmatrix}\Delta P_\infty \\ \Delta Q_\infty\end{bmatrix} \quad (20)$$

$$\Delta E_g = \frac{1}{A_1B_2 - A_2B_1}\ (B_2\Delta P_\infty - A_2\Delta Q_\infty) \quad (21)$$

$$\Delta E_g = G_1 \Delta P_\infty + G_2 \Delta Q_\infty) \quad (22)$$

Where;

$$G_1 = \frac{B_2}{A_1B_2 - A_2B_1}$$

$$G_2 = \frac{-A_2}{A_1B_2 - A_2B_1}$$

$$\Delta\delta = \frac{1}{A_1B_2 - A_2B_1}\ (-B_1\Delta P_\infty + A_1 \Delta P_\infty) \quad (23)$$

$$\Delta\delta = G_3 \Delta P_\infty + G_4 \Delta Q_\infty) \quad (24)$$

Where;

$$G_3 = \frac{-B_1}{A_1B_2 - A_2B_1}$$

$$G_4 = \frac{A_1}{A_1B_2 - A_2B_1}$$

From the complete analysis of proposed mathematical model, the APF at infinite bus can be controlled by the input parameters of governor position and field voltage while maintaining the reactive power constancy.

4. OPTIMIZATION PARAMETERS OF REALITY SYSTEM

Many researchers have interested with the FSTPID controller to realize better response over voltage and frequency deviations in power system [23], [24]. The structure of OFSTPID controller is divided into two parts:

4.1 Controller parameters optimization

The 6th parameters of PID controller of the active control loop (k_{p_P}, k_{i_P}, k_{d_P}) and reactive control loop (k_{p_Q}, k_{i_Q}, k_{d_Q}) are optimized by the ACO method. The method of ACO has an effective solution in short time, an acceptable solution due to greedy heuristic of searching process and the early convergence is avoided during the distributed computation [25].The optimization process based on the global objective function(F_g). It can be expressed as:

$$F_g = F_1 + F_2 + F_3 + F_4 \quad (25)$$

The different objective functions$F_1, F_2, F_3$and $F_4$are represented as:

- Error minimization between desired and actual value of the active power demand over all the simulation time from 0:70 second. The integral square error (e_P) of active power loop is minimized by the form of equation (26).

$$F_1 = \int_0^t e_P^2(t)\,.\,dt \quad (26)$$

- The objective function in equation (27) represents the minimization parameters of active power control loop which represent the rise time (t_{r_P}), over shoot (O_{s_P}), settling time (t_{s_P}) and steady state error (e_{ss_P}). The dynamic parameters are weighted by scaling factors $\propto_P, \beta_P, \gamma_Pand\delta_P$. The scaling factors are arbitrarily selected to enforce the priority of each individual objective.

$$F_2 = \frac{1}{[\propto_P(t_{r\_P} - t_{r\_m\_p}) + \beta_P(O_{s\_P} - O_{s\_m\_p}) + \gamma_P(t_{s\_P} - t_{s\_m\_p}) + \delta_P(e_{ss\_P} - e_{ss\_m\_p})]} \quad (27)$$

Where $t_{r_m_p}, O_{s_m_p}, t_{s_m_p}ande_{ss_m_p}$are the rise time measurement, over shoot measurement, settling time measurement and steady state error measurement of the active power control loop respectively.

- Error minimization between desired and actual value of the reactive power demand over all the simulation time from 0:70 second. The integral square error (e_Q) of reactive power loop is minimized by the form of equation (28).

$$F_3 = \int_0^t e_Q^2(t)\,.\,dt \quad (28)$$

- The objective function in equation (29) represents the minimization parameters of active power control loop which represent the rise time (t_{r_P}), over shoot (O_{s_P}), settling time (t_{s_P}) and steady state error (e_{ss_P}). These parameters are weighted by scaling factors $\propto_Q, \beta_Q, \gamma_Qand\delta_Q$. The scaling factors are arbitrarily selected to enforce the priority of each individual objective. The flowchart of ACO algorithm to optimize the controller parameters (PID) shown in Fig. 5.

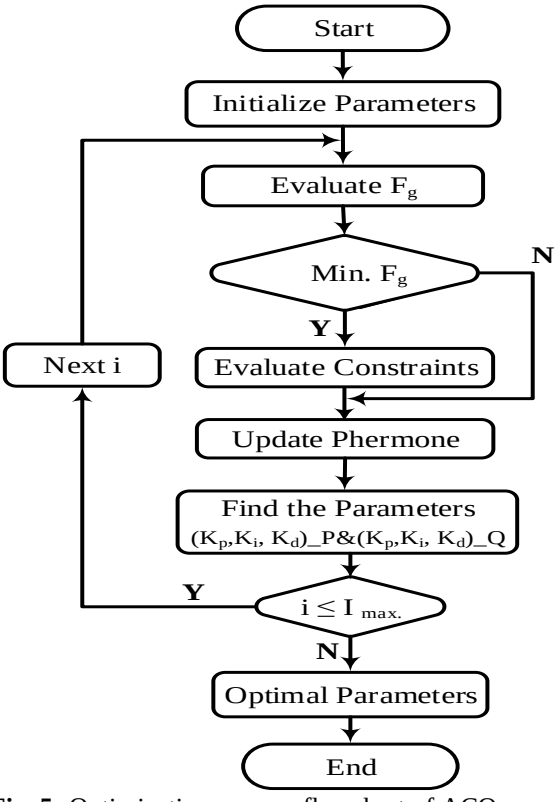

Fig. 5: Optimization process flowchart of ACO

$$F_4 = \frac{1}{[\propto_Q(t_{r\_Q} - t_{r\_m\_Q}) + \beta_Q(O_{s\_Q} - O_{s\_m\_Q}) + \gamma_Q(t_{s\_Q} - t_{s\_m\_Q}) + \delta_Q(e_{ss\_Q} - e_{ss\_m\_Q})]} \quad (29)$$

4.2 Determination of control parameters based on fuzzy rules

The second part relies on updating the control response by FSTPID controller to adjust the gains of two control loops to improve the performance of reality power system through the load disturbance. The output of fuzzy controller is responsible for correction the control action related to the error (e), the change of error (Δe) as shown in Fig. 6 and the rule base structure between them depicted in Table 1.

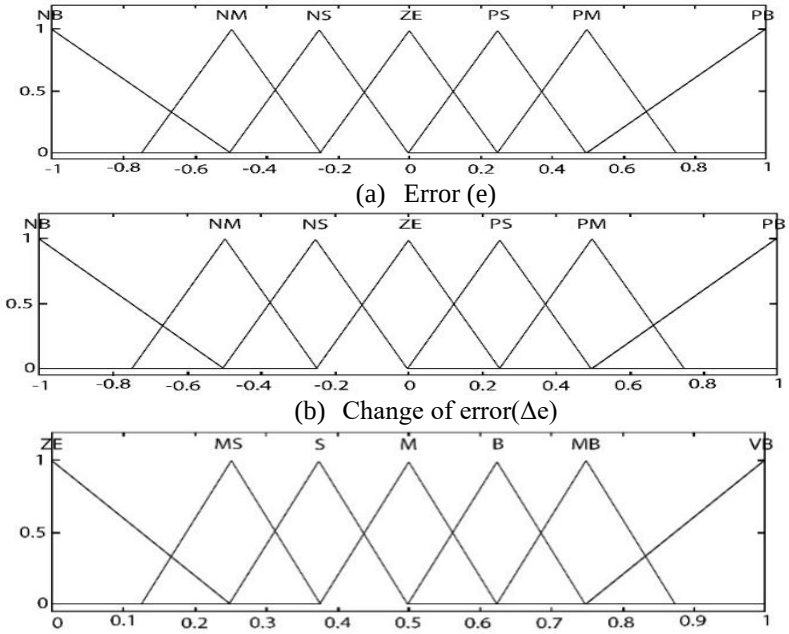

(a) Error (e)

(b) Change of error(Δe)

(c) Output membership function of FLC

Fig. 6 Inputs and output membership functions of FLC

Table 1: Rule Base structure of FLC

a- K_{PF}

Δe / e	N B	NM	N S	Z E	P S	P M	P B
N B	V B	V B	V B	V B	V B	V B	V B
NM	MB	MB	MB	MB	B	MB	V B
N S	B	B	B	B	MB	B	V B
Z E	Z E	Z E	Z E	M S	S	S	S
P S	B	B	B	B	MB	B	V B
P M	MB	MB	MB	MB	B	MB	V B
P B	V B	V B	V B	V B	V B	V B	V B

b- K_{IF}

Δe / e	N B	NM	N S	Z E	P S	P M	P B
N B	M	M	M	M	M	M	M
N M	M	M	M	M	M	M	M
N S	S	S	S	S	S	S	S
Z E	MS	MS	MS	Z E	MS	M S	MS
P S	S	S	S	S	S	S	S
P M	M	M	M	M	M	M	M
P B	M	M	M	M	M	M	M

c- K_{DF}

Δe / e	NB	N M	N S	Z E	P S	P M	PB
N B	Z E	M S	S	M	MB	B	VB
NM	MS	S	M	B	B	B	VB
N S	S	M	B	MB	V B	VB	VB
Z E	M	B	MB	MB	V B	VB	VB
P S	MB	MB	V B	V B	V B	VB	VB
P M	B	MB	V B	V B	V B	VB	VB
P B	V B	MB	V B	V B	V B	VB	VB

The total output control action of FSTPID is illustrated in Fig.7 and represented by the equation (30) [12].

$$U_{tun} = K_{P\_tun} + K_{I\_tun} \int edt + K_{D\_tun} \frac{de}{dt} \quad (30)$$

Where, U_{tun} is the total output control action of FSTPID, $K_{P\_tun} = K_P * K_{PF}$, $K_{I\_tun} = K_I * K_{IF}$ and $K_{D\_tun} = K_D * K_{DF}$.

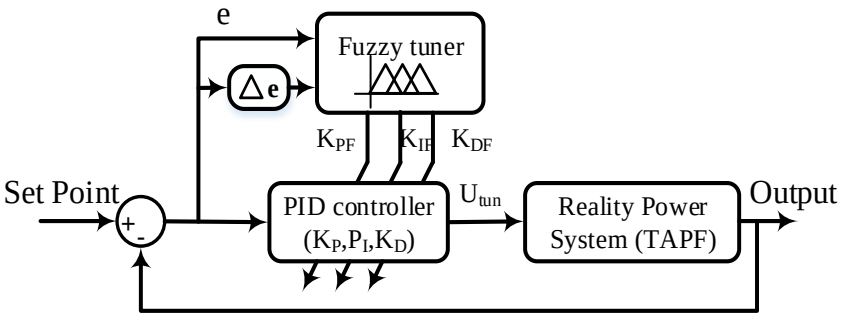

Fig. 7: Structure of FSTPID.

The defuzzification process is responsible to produce the gains (K_{PF}, K_{IF} and K_{DF}) by converting the fuzzy output to crisp values based on the center of gravity equation (31).

$$u = \frac{\sum_{i=1}^{r} u(u_i)u_i}{\sum_{i=1}^{r} u(u_i)} \quad (31)$$

Where $u(u_i)$ is the weight of membership the element (u_i) which is the output of the rule.

5. RESULTS AND DISCUSSIONS

We will discuss the final simulation results of the proposed tracking APF/RPF method for both PID controller and OFSTPID controller in the presence of the same APF disturbances. In Fig.8a, the APF response has been tracked the active power demand value for each controller in two control strategies. But, the response of OFSTPID controller is better than PID controller response during the positive and negative APF disturbances during 5-20 seconds and 35-50 seconds. The settling time of OFSTPID controller during positive and negative APF disturbance is1.1 second while of the PID controller is 12.23 second. The peak overshoot of two methods as the same percentage at 12.5%. The OFSTPID controller has not peak undershoot while the PID controller method has a peak undershoot at 12.5 %.

The governor valve position response of OFSTPID controller illustrated in Fig. 9ahas a settling time of 0.7 seconds with peak overshoot (8%) and has not peak undershoot. While the governor valve position response of PID controller, the settling time is 12.2 seconds with peak overshoot (25%) and peak undershoot (-12%). In Fig.9b, there is a very important note that discriminates the OFSTPID controller according to PID controller. During the positive APF disturbance, the power angle of OFSTPID increased to 50.66^0 (8.69%). While, the power angle of PID controller increased to 53.2^0 (14.1%) for the same interval. Also, the power angle of OFSTPID decreased to 42.44^0 (8.94%) during the negative APF disturbance. While, the power angle of PID controller decreased to 40.75^0(12.6%) in the same interval. The power angle difference between two systems gives a relative advantage for proposed OFSTPID system by generating the same APF to the grid at certainpower anglesmaller than the power angle of PID controller. This means that the OFSTPID controller can be delivered greater APF than the of PID controller.Fig.9c shows the settling time of frequency deviation response of OFSTPID controller is 0.7 seconds with peak overshoot (0.006Hz) and does not peak undershoot. While the frequency deviation response of PID controller, the settling time is 9.8 seconds with peak overshoot (0.008 Hz) and peak undershoot (-0.0002Hz).

Also, the RPF response in Fig.10ahas been tracked the reactive power demand value for each controller in two control strategies. But, the response of OFSTPID controller is better than PID controller response during the positive and negative RPF disturbances through 5-20 seconds and 35-50 seconds. The settling time of proposed method during positive and negative RPF disturbance is 2.1 second while the LFC is 10 second. The peak overshoot of proposed method is (30%pu) and without peak overshoot for conventional LFC. While, the OFSTPID and PID controllers have the same peak undershoot (-1%pu).

The exciter field voltage response of OFSTPID controller illustrated in Fig. 11a has a settling time of 0.5 seconds with peak overshoot (46%pu) and peak undershoot(27%pu). While the exciter field voltage response of PID controller has a settling time of 5.3 seconds without peak overshoot and peak undershoot. Although the overshoot and undershoot of OFSTPID controller greater than the response of PID controller but it's the range of allowable limits of field voltage.

The terminal voltage response of OFSTPID controller depicted in Fig. 11b has a settling time of 0.7 seconds with peak overshoot (0.04%pu) and peak undershoot (0.02%pu). While the terminal voltage response of PID controller has a settling time of 10.2 seconds with peak overshoot and peak undershoot (0.02%pu).

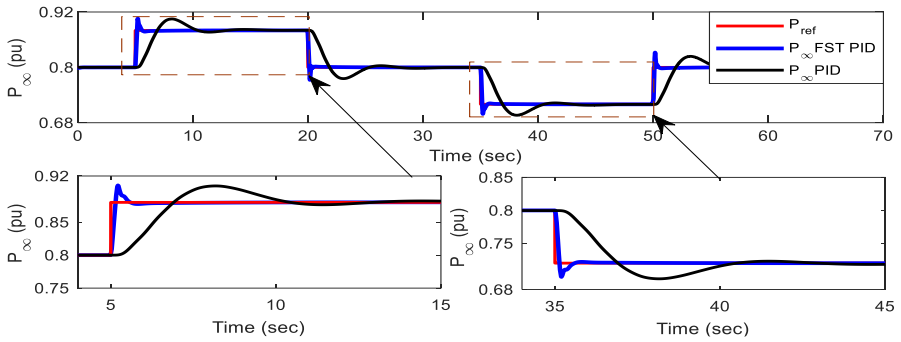

Fig. 8 APF output response of proposed system for PID and OFSTPID controllers

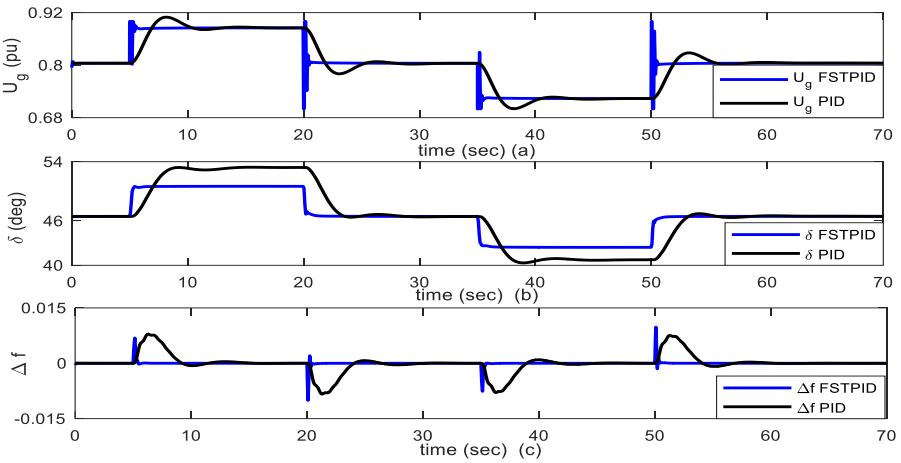

Fig. 9 Related output response of the APF of proposed system for PID and OFSTPID controllers. a- U_g; b- δ; c-Δf.

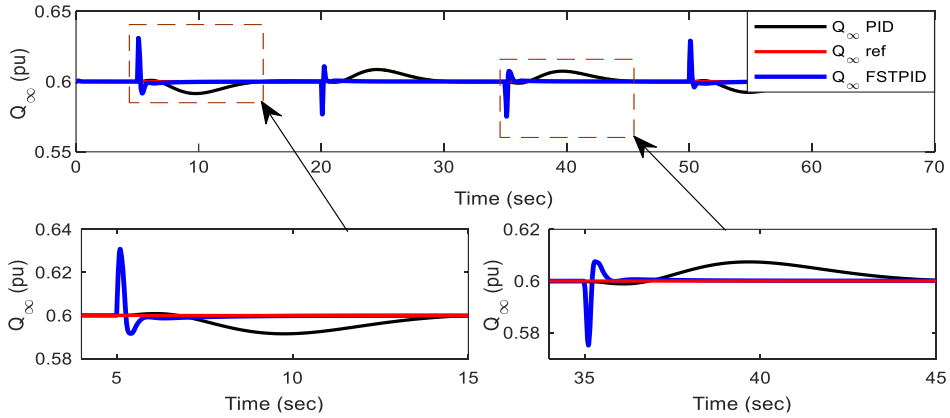

Fig. 10 RPF output response of proposed system for PID and OFSTPID controllers

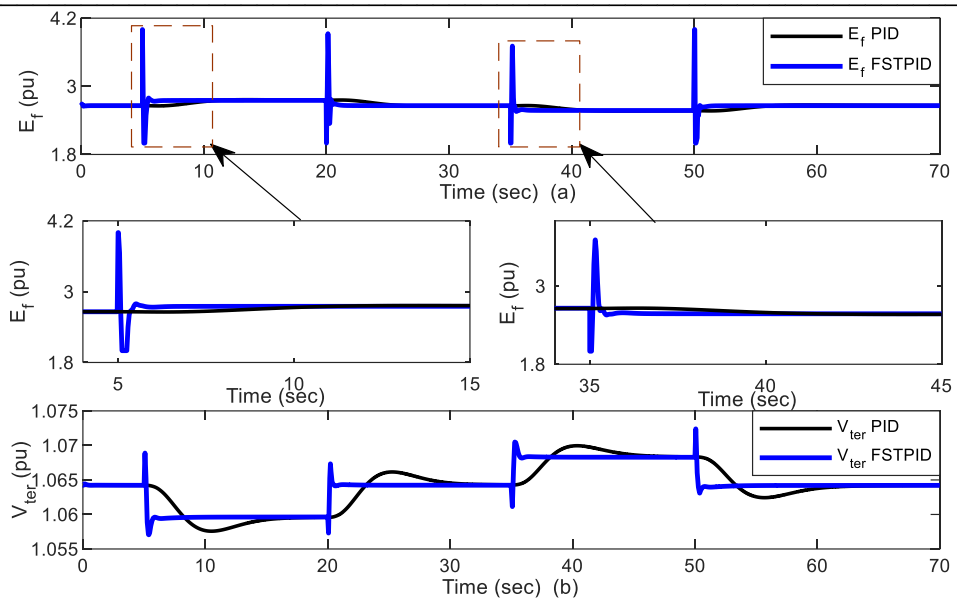

Fig. 11 Related output response of the RPF of proposed system for PID and OFSTPID controllers. a- E_f; b- V_{ter}.

Table 2 shows the differences between the recent publication work and the proposed methodology according to frequency deviation dynamic response. The comparison has been offered in transparency the differences of settling time (T_s), peak overshoot (M_P), peak time (T_p) and peak undershoot (U_P) during the +ve active load disturbance during the interval of +veAPFdisturbance of 0.08pu.The comparative study has been proved that the resultofproposed method is better than results of the related publicationworks in all dynamic parameters rather than maximum overshoot and peak undershoot in reference [30].But, the response of that reference was validated at load disturbanceΔP=0.02pu and settling time is 36.5 times the related value of the proposed method. Also, the load disturbancein the proposed method ΔP=0.08pu which represents four times the load disturbance in reference [30].

Table 2: Comparison between previous and proposed work

Ref.	Year	Control Method	ΔP (pu)	Cont. tech.	Δf (Hz)			
					T_s (Sec)	M_P (Hz)	T_P (Sec)	U_P (Hz)
[27]	2017	PI-Observer	0.01	LFC	8	0.1	1.5	-0.06
		Luenberger Observer	0.01		8	0.1	1.5	-0.05
[28]	2022	GA-PID	0.01	LFC+AVR	4.29	0.045	3	-1.5
		GA-PID	0.02		13.986	0.079	4.5	-3.2
		GWO-PID	0.05		15.294	0.162	7.5	-11.1
[26]	2019	NLTA-PID	0.02	AVR+LFC	0.74	1.34	0.23	NA
[29]	2022	PID	0.02	LFC	20.33	0.0014	10	- 0.005
		Classical. V .rot			16.4	0.0012	9.5	- 0.005
		Adap. V .rot			14.6	0.001	9	- 0.004
		PID	0.1		86.332	-	-	- 0.006
		Classical. V .rot			67.2850	0.003	12	- 0.006
		Adap. V .rot			57.452	0.0018	7	- 0.006
[30]	2017	PI-LFC	0.01	LFC	18	0.0002	3.5	-0.0028
		LMI-LFC			25	0.002	10	-0.0029
		LMI-NPLFC			15	0.001	7	-0.0029
		LMI-PLFC			13	0.0002	7	-0.0024
[31]	2023	FPIDD^2	0.01	LFC	13.8	0.003	5.5	-0.018
Proposed Control	2023	G_1, G_2, G_3 and G_4+ OFSTPID	0.08	Tracking of APF&RPF	0.4	0.0067	0.15	-0.005

Ts: Settling Time (±2% band); MP: Maximum Overshoot; TP: Peak Time; UP: Maximum Undershoot.

7. CONCLUSION

In the submitted paper, the control of APF and the RPF of turbo-generator system was studied through a new approach based on controlling both the governor valve position and exciter field voltage. it has been derived the correlation between the variations of active and reactive power delivered By finding four parameters (G_(1,) G_(2,) G_3 and G_4). These parameters are added to the control loops of governor valve position and exciter field voltage to control flow of active and reactive power and improve the system performance. the 6th parameters of FSTPID controllers are optimized for each control loop of governor volve position and exciter field voltage. The performance of the proposed

control method is compared with published related works according to system dynamics of frequency deviation. The comparison study shows that the superiority of proposed technique. As well as, the power angle in case of FSTPID (50.66o) is smaller than in case of conventional LFC (53.220) at the same load requirements which about (± 5% for increasing/decreasing APF). This means that, the synchronous generator has the ability to send larger active power for our proposed method.

The recommended future work is to apply the same conceptual analysis of reality power system when the active and reactive power load variation simultaneously.

REFERENCES

[1]. A. E. Salem, S. H. Arafah, and O. M. Salim, "Power quality enhancement of grid-islanded parallel microsources using new optimized cascaded level control scheme," Int. J. Electr. Power Energy Syst., vol. 140, p. 108063, 2022.

[2]. A. E. Salem, S. H. Arafah, and O. M. Salim, "Power quality enhancement of grid-islanded parallel microsources using new optimized cascaded level control scheme," Int. J. Electr. Power Energy Syst., vol. 140, no. September 2021, p. 108063, 2022, doi: 10.1016/j.ijepes.2022.108063.

[3]. V. P. Singh, N. Kishor, and P. Samuel, "Improved load frequency control of power system using LMI based PID approach," J. Franklin Inst., vol. 354, no. 15, pp. 6805–6830, 2017, doi: 10.1016/j.jfranklin.2017.08.031.

[4]. H. F. Sindi, S. Alghamdi, M. Rawa, A. I. Omar, and A. H. Elmetwaly, "Robust control of adaptive power quality compensator in Multi-Microgrids for power quality enhancement using puzzle optimization algorithm," Ain Shams Eng. J., p. 102047, 2022.

[5]. L. Yin, C. Zhang, Y. Wang, F. Gao, J. Yu, and L. Cheng, "Emotional deep learning programming controller for automatic voltage control of power systems," IEEE Access, vol. 9, pp. 31880–31891, 2021.

[6]. C. H. N. S. Kalyan et al., "Comparative Performance Assessment of Different Energy Storage Devices in Combined LFC and AVR Analysis of Multi-Area Power System," Energies, vol. 15, no. 2, p. 629, 2022.

[7]. C. H. Kalyan and G. S. Rao, "Impact of communication time delays on combined LFC and AVR of a multi-area hybrid system with IPFC-RFBs coordinated control strategy," Prot. Control Mod. Power Syst., vol. 6, no. 1, pp. 1–20, 2021.

[8]. M. Bhuyan, D. Chandra Das, and A. Kumar Barik, "Combined voltage and frequency response in a solar thermal system with thermostatically controlled loads in an isolated hybrid microgrid scheme," Int. J. Sustain. Energy, pp. 1–24, 2022.

[9]. K. R. M. V. Chandrakala and S. Balamurugan, "Simulated annealing based optimal frequency and terminal voltage control of multi source multi area system," Int. J. Electr. Power Energy Syst., vol. 78, pp. 823–829, 2016.

[10]. D. K. Lal and A. K. Barisal, "Combined load frequency and terminal voltage control of power systems using moth flame optimization algorithm," J. Electr. Syst. Inf. Technol., vol. 6, no. 1, pp. 1–24, 2019.

[11]. R. Rajbongshi and L. C. Saikia, "Combined control of voltage and frequency of multi-area multisource system incorporating solar thermal power plant using LSA optimised classical controllers," IET Gener. Transm. Distrib., vol. 11, no. 10, pp. 2489–2498, 2017.

[12]. N. Jalali, H. Razmi, and H. Doagou-Mojarrad, "Optimized fuzzy self-tuning PID controller design based on Tribe-DE optimization algorithm and rule weight adjustment method for load frequency control of interconnected multi-area power systems," Appl. Soft Comput., vol. 93, p. 106424, 2020.

[13]. H. Anantwar, D. B. R. Lakshmikantha, and S. Sundar, "Fuzzy self tuning PI controller based inverter control for voltage regulation in off-grid hybrid power system," Energy Procedia, vol. 117, pp. 409–416, 2017, doi 0.1016/j.egypro.2017.05.160.

[14]. M. Taghdisi and S. Balochian, "Maximum power point tracking of variable-speed wind turbines using self-tuning fuzzy PID," Technol. Econ. Smart Grids Sustain. Energy, vol. 5, no. 1, pp. 1–8, 2020.

[15]. A. Naderipour, Z. Abdul-Malek, I. F. Davoodkhani, H. Kamyab, and R. R. Ali, "Load-frequency control in an islanded microgrid PV/WT/FC/ESS using an optimal self-tuning fractional-order fuzzy controller," Environ. Sci. Pollut. Res., 2021, doi: 10.1007/s11356-021-14799-1.

[16]. C. Mu, Y. Tang, and H. He, "Improved sliding mode design for load frequency control of power system integrated an adaptive learning strategy," IEEE Trans. Ind. Electron., vol. 64, no. 8, pp. 6742–6751, 2017.

[17]. H. Haes Alhelou, M. E. Hamedani-Golshan, R. Zamani, E. Heydarian-Forushani, and P. Siano, Challenges and opportunities of load frequency control in conventional, modern and future smart power systems: A comprehensive review, vol. 11, no. 10. 2018. doi: 10.3390/en11102497.

[18]. N. R. Babu et al., A Comprehensive Review of Recent Strategies on Automatic Generation Control / Load Frequency Control in Power Systems A Comprehensive Review of Recent Strategies on Automatic

Generation Control / Load Frequency Control in Power Systems, no. September. Springer Netherlands, 2022. doi: 10.1007/s11831-022-09810-y.

[19]. T. Ali, S. A. Malik, A. Daraz, M. Adeel, S. Aslam, and H. Herodotou, "Load Frequency Control and Automatic Voltage Regulation in Four-Area Interconnected Power Systems Using a Gradient-Based Optimizer," Energies, vol. 16, no. 5, 2023, doi: 10.3390/en16052086.

[20]. V. Kumar, V. Sharma, and R. Naresh, "HHO-based Model Predictive Controller for Combined Voltage and Frequency Control Problem Including SMES," IETE J. Res., 2021, doi: 10.1080/03772063.2021.1908180.

[21]. M. Alharbi et al., "Innovative AVR-LFC Design for a Multi-Area Power System Using Hybrid Fractional-Order PI and PIDD2 Controllers Based on Dandelion Optimizer," Mathematics, vol. 11, no. 6, p. 1387, 2023, doi: 10.3390/math11061387.

[22]. A. Zaporozhets and V. Artemchuk, Systems, Decision and Control in Energy II, vol. 346. 2021. [Online]. Available: http://link.springer.com/10.1007/978-3-030-69189-9

[23]. J. R. Nayak, B. Shaw, B. K. Sahu, and K. A. Naidu, "Application of optimized adaptive crow search algorithm based two degree of freedom optimal fuzzy PID controller for AGC system," Eng. Sci. Technol. an Int. J., vol. 32, p. 101061, 2022, doi: 10.1016/j.jestch.2021.09.007.

[24]. T. Dogruer and M. S. Can, "Design and robustness analysis of fuzzy PID controller for automatic voltage regulator system using genetic algorithm," Trans. Inst. Meas. Control, vol. 44, no. 9, pp. 1862–1873, 2022, doi: 10.1177/01423312211066758.

[25]. V. Kumarakrishnan, G. Vijayakumar, D. Boopathi, K. Jagatheesan, S. Saravanan, and B. Anand, Frequency Regulation of Interconnected Power Generating System Using Ant Colony Optimization Technique Tuned PID Controller, vol. 822. 2022. doi: 10.1007/978-981-16-7664-2_11.

[26]. N. Nahas, M. Abouheaf, A. Sharaf, and W. Gueaieb, "A Self-Adjusting Adaptive AVR-LFC Scheme for Synchronous Generators," IEEE Trans. Power Syst., vol. 34, no. 6, pp. 5073–5075, 2019, doi: 10.1109/TPWRS.2019.2920782.

[27]. A. A. Hussein, S. S. Salih, and Y. G. Ghasm, "Implementation of Proportional-Integral-Observer Techniques for Load Frequency Control of Power System," Procedia Comput. Sci., vol. 109, pp. 754–762, 2017, doi: 10.1016/j.procs.2017.05.307.

[28]. N. Paliwal, L. Srivastava, and M. Pandit, "Application of grey wolf optimization algorithm for load frequency control in multi-source single area power system," Evol. Intell., vol. 15, no. 1, pp. 563–584, 2022, doi: 10.1007/s12065-020-00530-5.

[29]. H. Abubakr, J. C. Vasquez, T. Hassan Mohamed, and J. M. Guerrero, "The concept of direct adaptive control for improving voltage and frequency regulation loops in several power system applications," Int. J. Electr. Power Energy Syst., vol. 140, no. February, p. 108068, 2022, doi: 10.1016/j.ijepes.2022.108068.

[30]. P. Ojaghi and M. Rahmani, "LMI-Based Robust Predictive Load Frequency Control for Power Systems with Communication Delays," IEEE Trans. Power Syst., vol. 32, no. 5, pp. 4091–4100, 2017, doi: 10.1109/TPWRS.2017.2654453.

[31]. A. A. Hossam-Eldin, E. Negm, M. Ragab, and K. M. AboRas, "A maiden robust FPIDD2 regulator for frequency-voltage enhancement in a hybrid interconnected power system using Gradient-Based Optimizer," Alexandria Eng. J., vol. 65, pp. 103–118, 2023, doi: 10.1016/j.aej.2022.10.029.